A Device for Rapid, Automated Trimming of Insect-Sized Flying Robots

Daksh Dhingra

A thesis
submitted in partial fulfillment of the
requirements for the degree of

Master of Science

University of Washington

2019

Committee:

Sawyer B. Fuller, Chair

Joseph Garbini

Eric Rombokas

Program Authorized to Offer Degree:
Mechanical Engineering

University of Washington

Abstract

A Device for Rapid, Automated Trimming of Insect-Sized Flying Robots

Daksh Dhingra

Chair of the Supervisory Committee:
Professor Sawyer B. Fuller
Mechanical Engineering

Successful demonstrations of controlled flight in flying insect-sized robots (FIRs) <500 mg have all relied on piezo-actuated flapping wings because of unfavorable downward size scaling in motor-driven propellers. In practice, the mechanical complexity of flapping wings typically results in large torque bias variability about pitch and roll axes, leading to rapid rotation in free flight for vehicles that are not properly trimmed. Manual trimming by watching high-speed video is tedious and error-prone. In this letter, we introduce an alternative, a trimming device that uses feedback from motion capture cameras to determine and correct for bias torques. It does so using an automated feedback loop, without the need for any visual feedback from the user, or airborne flights which can damage the robot. We validated the device on two different robot flies. After trimming with our device, the robots both took off approximately vertically in open-loop and were able to hover in free flight. Our system, therefore, speeds up an essential yet time-consuming step in robot fly fabrication, facilitating their eventual mass production and practical application.

TABLE OF CONTENTS

LIST OF FIGURES

LIST OF TABLES

GLOSSARY

BIAS TORQUE: A torque inherent to a robot which causes it to have some attitude during initial flight. This is generally introduced due to manufacturing inconsistencies in the robot.

TRIM TORQUE: A value of torque that counteracts the bias torque. These are generated by a specific set of trim values, in our case it is voltage offset (V_{offset}) and amplitude differential (δA).

ROBOFLY-EXPANDED: This is the name of our robot. It is an improved version of Robofly and is used in all the experiments in this thesis.

TRIMMING DEVICE: A devie developed in this thesis used for finding the trim values.

FLYING INSECT ROBOT (FIR) : Name used to refer a class of airborne robots that are of inset scale. Robofly-Expanded is an example of one such robot.

FLEXURE JOINTS: These joints connect two rigid links with an elastic member. This allows a relative rotation between the rigid links about the elastic member.

MOTION CAPTURE SYSTEM (MOCAP): This is a system used to record the movements of objects using tracking cameras. In this research MoCap is used to track the attitude and position of Robofly-Expanded.

ACKNOWLEDGMENTS

I am extremely grateful to my advisor Dr. Sawyer Fuller, who helped me at every step during this research. He originally came up with the idea for my thesis and advised me until its completion. His unparalleled support and insightful suggestions guided me through the problems we faced along the way.

I would also like to extend my deepest gratitude to my labmate Yogesh Chukewad. He played an instrumental role in the experiments performed on the Robofly.

I would like to thank my thesis committee Dr. Joseph Garbini and Dr. Eric Rombokas for their insightful discussions and suggestions.

I would also like to acknowledge the consistent support of my lab mates at the Autonomous Insect robotics lab. They gave me practical suggestions and maintained a positive environment in the lab.

I am forever grateful to my parents, my sister and my brother in law. They were with me at every step along the way. This wouldn't have been possible without them.

DEDICATION

To my sister, Priyanka.

Chapter 1
INTRODUCTION

1.1 Motivation

Due to their small size and ability to explore confined spaces, flying insect-sized robots (FIRs) can be used in search and rescue missions. They are inexpensive and extremely lightweight—with a mass measured in milligrams—making them an appealing alternative to large rovers for space exploration. We can potentially send thousands of these robots in space at very low cost for expeditions and data gathering. They might also be used for crop monitoring in farming applications. The motivation is to someday mass produce these at low cost like electronic chips which is perfect for use in dangerous environments where they might get damaged.

With the decline in bee population many varieties of fruits and vegetables can come to an end. We need ways to pollinate plants without them. Due to their light weight and small size FIRs are viable alternatives to pollinate flowers or plants in future.

1.2 Background

The first feedback-controlled flying insect robot (FIR) was demonstrated in [2]. Since then, improvements to the basic design have explored increasing payload capacity, simplifying fabrication, and achieving passive attitude stability. In [3] the effect of relative position between the aerodynamics center and center of gravity on intrinsic attitude stability of the FIR was studied, and [4] provided better understanding of dynamics of a flapping wing mechanism. In [5] a four-wing design with increased payload capacity and steering actuation was demonstrated, this work also elucidated the controller design for FIRs. It focused on the adaptive component used to control four wing robots which is important in robots with flapping wing mechanism due error in thrust vector direction because of manufacturing uncertainties. [6] introduced an alternative design ac-

tuated by uniomorph actuators. To expand the mobility of robot flies, [1] improved the design by reducing part count and lowering the center of mass, allowing landing and ground ambulation in addition to flight. An emerging alternative to flapping wings also suited to insect scale is miniaturized electrohydrodynamic thrust introduced in [7] and [8].

Each of the foregoing FIR flight demonstrations required that the robot be trimmed, regardless of the number of actuators or design of the robot. From undergraduate physics, an arbitrary set of forces and torques acting on a rigid body can be decomposed into a single force vector acting at its center of mass, and a torque vector. For flight control, we can make two statements about the force and torque acting on a properly-trimmed hovering device such as the Robofly [1]:

1. A zero commanded torque should result in zero net rotational acceleration.

2. A thrust force should result in a zero net lateral acceleration in the body frame.

Here, we are primarily concerned with (1) above, because a non-zero bias torque results in much larger flight path deviations, which make it hard to correct for in free-flight.

In the context of small flapping-wing robots like FIRs, trimming at such small scales entails two challenges that distinguish it from larger vehicles: (1) Rotational acceleration rates increase as size scale diminishes [9, 10], making the dynamics of small vehicles particularly fast. The challenge is exacerbated by the fact that, like many flying insects including fruit flies and hawkmoths, their dynamics are unstable [4, 11, 10]. And (2) being based predominantly on flapping wings, FIRs consist of a flapping mechanism that, by virtue of its novelty, small size, and complexity, is subject to greater variability in performance than, for example, slightly larger quad-rotor helicopters. The result is that the magnitude of compensatory trim required is larger. As a result, in almost all cases, the first open-loop flights of such robots without trimming result in rapid inversion and a subsequent crash. If the vehicle does take off, it typically moves too far—out of the range of tracking cameras—before the controller is able to adapt for and correct for this irregularity. The trimming device we introduce in this work addresses both challenges.

1.3 Main Contribution

For this work, we define the torque trimming process to be the task of finding a trim torque, τ_t, that exactly cancels the non-zero bias torque τ_b. A bias torque τ_b can arise from a) manufacturing inconsistencies, b) wear, and c) if there is damage to the FIR. The bias torque varies from robot to robot, as well as with changes in the payload carried by the robot, like a camera [12], boost converters for onboard power in [13], or an array of photovoltaic cells in [14], making trimming necessary for each robot. In current practice [15, 16, 5, 1], trimming was performed by filming short flights $<$0.5 s using a high speed camera. The magnitude and direction of the bias torque vector were estimated manually by observing the slow-motion videos. This method requires many human handled, unstable, and thus crash-prone flights.

In this thesis, we introduce a new purpose-designed apparatus [17] that can trim FIRs precisely, rapidly, and automatically. In addition to reducing the operator time it takes to trim a robot, our trimming device reduces the amount of wear and tear on the robot. In comparison, trimming using open-loop takeoffs from the ground invariably involves impacts to the wings, and requires manual handling to re-right the vehicle, which often entails an even greater chance of damage. It is also possible to trim a vehicle hanging from a thin kevlar filament, eliminating wing impacts, but this brings its own set of problems including damage when the wing becomes entangled in this filament, and it is often difficult to disambiguate, in video footage, torques due to torque baises versus those arising from tension on the filament.

In our device, trimming is performed through closed-loop feedback. While the wings are flapped, a controller receives Euler Angles in real-time and continuously updates trim values to counteract bias torques. In particular, the device allows us to minimize two quantities: the pitch bias torque τ_b^{pitch} and the roll bias torque τ_b^{roll}. After doing so, the robot lifts off nearly vertically. This effectively places the flying system's state within the stability basin of our closed-loop free-flight controller. In the remainder of this report we describe the design, operation, and testing of this new apparatus.

Chapter 2

TRIMMING

2.1 Principles of Operation

The concept of trimming was first introduced in the ships [18] for achieving desired velocity and direction. This term was later adapted by the aviation community to indicate the process of moving on-board freight and trim tabs to achieve a stable flight condition. Trim analysis is a very fundamental and essential procedure in flight mechanics. Formally defined in [19], trim is a flight condition in which the rate of change of the state vector of an aircraft is zero when there are no net applied forces and moments. This definition holds a different significance depending on the type of air vehicle. In helicopters, [20] trimming analysis is a vital part of a stable flight and mid-air maneuvering, this is achieved by using three independent control inputs for the main rotor and one for the tail rotor . In airplanes, trim tabs are provided to a pilot for adjusting stick and rudder paddle forces [19]. In quad-rotor helicopters, pitch and roll trim is typically performed by adjusting the relative speeds of the rotors to compensate for weight or thrust imbalance. In FIRs, trimming consists of altering the wing kinematics so that there is zero net torque applied.

2.1.1 Dynamics analysis of an untrimmed flight

To understand the relevance of trimming analysis in FIRs, we will consider the trajectory of an untrimmed robot controlled by attitude and altitude controller in a 2-dimensional plane, actuated by a thruster on either side. The thrusters can be wings, motors or any source of producing upward thrust. We simulate the robot under the condition that it has a non-zero bias torque on its pitch axis. The parameters used for the simulations are obtained from Robofly-Expanded, given in table 2.1; more details on the robot are presented in a later section.

The robot is simulated as a 3 degree of freedom system with state vector $q = [\theta\ \dot{\theta}\ x_w\ z_w\ \dot{x}_w\ \dot{z}_w]$.

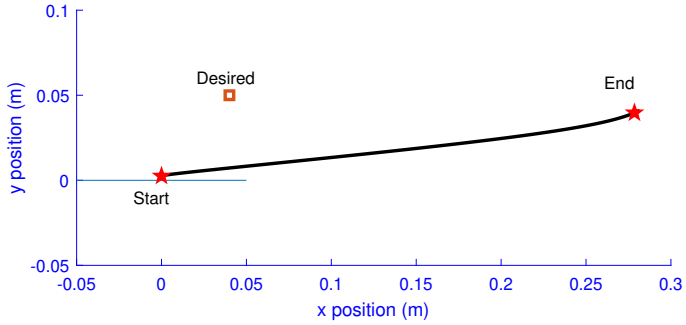

Figure 2.1: Simulated trajectory (in black) of an untrimmed flight being controlled by an attitude and an altitude controller in MATLAB. The attitude of the robot stabilizes outside the control volume of motion capture arena due to a high initial bias torque. The red square is the desired position of robot.

Here, θ is the angle and $\dot{\theta}$ is the angular velocity of the robot in the body coordinate system. x_w, z_w , $\dot{x}_w$, and $\dot{z}_w$ are position and velocity of the robot in world coordinate system. Body dynamics in this system are represented by Eq. 2.1. Because the wing amounts to 1% of body mass, we neglect the gyroscopic effect of wing inertial dynamics in our model.

$$\begin{aligned} m\ddot{x}_b &= -mg\sin\theta - m\dot{\theta}\dot{z}_b - b_w\dot{x}_b - b_w\dot{\theta}r_w \\ m\ddot{z}_b &= -mg\cos\theta - m\dot{\theta}\dot{x}_b - b_w\dot{z}_b + u_1 \\ J\ddot{\theta} &= r_w^2 b_w\dot{\theta} - r_w b_w\dot{x}_b + u_2 - \tau_b \end{aligned} \tag{2.1}$$

Here x_b and z_b are positions in body coordinates, which are used to obtain x_w, z_w , $\dot{x}_w$, and $\dot{z}_w$, b_w is the experimental value of aerodynamic drag on the wings [11], obtained from wind tunnel tests, r_w is the distance between centre of mass of the robot COM_R and aerodynamic centre (AC) which is approximately 3 mm for Robofly-Expanded, and u_1 and u_2 are the control force and control moment, generated from altitude and attitude controller respectively. The drag force components in X and Z, acting at AC, are proportional to the velocity at that point. These forces are translated to COM and are represented by b_w terms in the Eqs. 2.1. The terms involving $\dot{\theta}$ in the first two sub-equations of Eq. 2.1 are fictitious forces generated by taking the derivative of velocity in the

Table 2.1: Parameters used for 2D simulation of a robot with initial bias torque in MATLAB.

Parameter	**Value**
Mass of the robot	120 mg
Moment of Inertia (J)	1.2×10^{-6} kgm^2
Bias torque (τ_b)	40×10^{-6} Nm
Aerodynamic drag (b_w)	2×10^{-4} Ns/m

body frame. We simulated this system using the ode45 solver in MATLAB with initial conditions $\theta = z_b = x_b = 0$ under typical conditions of pitch torque bias τ_b of 40 μNm. This value is obtained using the frames of a high speed video of Robofly-Expanded without any trim compensation. The simulation predicts that under these conditions, the robot moves a long distance, more than 20 cm before its position reaches equilibrium (Fig. 2.1). Moving this far is undesirable because it may be larger than the tracking volume of a motion capture system, or will lead to impacts with obstacles. A trimming system that can measure such biases so that they can be compensated for before the first free flights can eliminate this hazard.

Trim plays an important role in a FIRs because: (1) A FIRs is inspired by flying insects like Drosophila and hawkmoths, and it inherits highly unstable and fast dynamics from its paradigms [4] [10], (2) the assembly of these robots involve manually folding and gluing of a lot of discrete parts under a microscope which results in some variations in each half of the robots, and (3) insect sized flapping wings robots are subjected to a lot of wear even in flight times as low as 5 to 10 minutes, which often warrants re-trimming. Due to all these reasons even a simple closed loop takeoff on a FIRs without trimming would result in an imminent crash or the robot can drift too far before the controller can step in.

2.2 Trimming About an Elastic Rotation Axis

Torque sensing is commonly achieved by measuring small rotational deflections. One approach is to create a rigid system with sensors capable of detecting small deflections, e.g. the Nano17 Titanium (ATI Industrial Automation, NJ, USA). While this provides high bandwidth, the 8 μNm resolution is insufficient. Capacitive pickup is an alternative that has demonstrated sufficient precision [21], but requires costly electronics hardware and has not been demonstrated in two axes. Our approach is to instead use a low-stiffness spring. This sacrifices unneeded bandwidth in exchange for large deflections that can be measured using sensors commonly available in a robotics laboratory such as a motion capture system or accelerometer, and can be built using the same processes used to fabricate the robot itself.

We begin by introducing the underlying physics of a flying robot attached to a trimming device of our design, whose basic form is shown in Fig. 2.2(b). The principle of operation relies on the fact that the device constrains the robot to rotate around a single axis while keeping all other degrees of freedom fixed. The axis is subject to a spring-like restoring torque so that the robot remains upright at equilibrium. In our device, there are two such axes—pitch and roll—so that both can be trimmed simultaneously. When the wings are flapped, they in general produce both a thrust and a torque. Our device is designed so that applied torque, such as an undesirable bias torque τ_b, results in a rotation in proportion to its magnitude. Whereas its design insures that thrust has no effect on rotation, regardless of magnitude. Trimming the robot then consists of determining the direction and magnitude of compensating trim torque τ_t that reduces rotation approximately to zero.

For our system to operate in this way, we must make the following assumptions about the thrust vector:

1. Its direction is vertical (coincident with the body-Z axis)

2. It is nearly collinear with the axis of rotation of the flexure joint (that is, the lateral offset O_R shown in Fig. 2.2 is small).

We will later show, in Section IIIC, how our device design includes a calibration process in

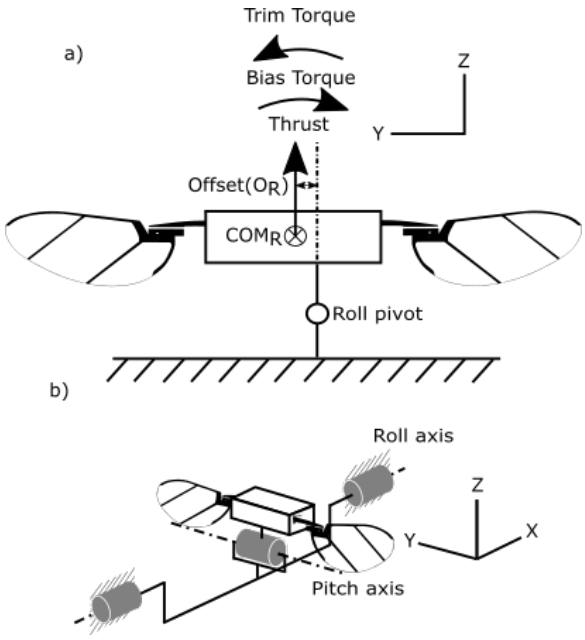

Figure 2.2: (a) A 2D representation of forces and torques acting on the robot attached to a single-axis version of the trimming device. The robot is constrained to rotate freely around a single axis; assuming O_R can be made small, the trim device rotates in response to a bias torque, which can be corrected by adding a compensatory trim torque. (b) A 3D representation of the rotation axes of the two-axis trimming device reported here, which allows trimming roll and pitch axes simultaneously.

which the robot is precisely positioned to insure assumption (3) above holds.

In our device, we use an integrating feedback control loop to find the compensatory trim torque τ_t. The dynamical equation for how the system's rotation angle evolves with time is:

$$J\ddot{\theta} = \tau_b - k_s\theta - c\dot{\theta} + \tau_t \tag{2.2}$$

Here J is the moment of inertia of the combined robot-trimming device system, θ is the rotation angle, τ_b and τ_t are the bias torque and trim torque respectively, k_s is a spring-like stiffness constant (derived below), and c is a rotational damping coefficient due to aerodynamic drag forces on the flapping wings and damping in the flexure joints. We can solve for the angle at steady-state, giving

$$\theta = \frac{1}{k_s}(\tau_b + \tau_t). \tag{2.3}$$

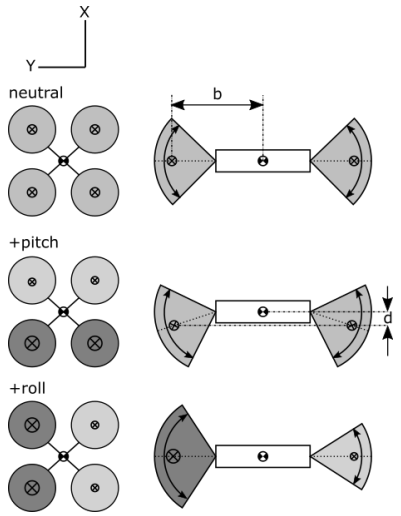

Figure 2.3: A comparison of the mechanisms by which quad-rotor aircraft and the Robofly actuate pitch and roll torques. The centers of aerodynamic thrust are denoted by a $\otimes$ with a size proportional to thrust magnitude

This shows that the only way to make the angle zero is to make $\tau_b = \tau_t$. This provides a means to determine that the robot is trimmed, without the need to know the exact value of k_s. Practical design considerations limit the range of k_s, which we address below. If we can measure the angle θ of the robot in the trimming device, for example by using a motion capture camera or an on-board accelerometer, then we can use an integral controller to integrate this error in time to drive it to zero:

$$\tau_t = k_i \int_0^t (\theta_d - \theta)\, dt, \tag{2.4}$$

where k_i is the integral controller constant and θ_d is the desired angle, which is zero in our case. This concept can be used for finding both roll and pitch trim torques.

2.3 Mechanisms of Torque Actuation

For torque trimming, we are not concerned with the exact mechanism by which a bias torque τ_b arises, but we must have the means to compensate for it using a trim torque τ_t. In both quad-rotor

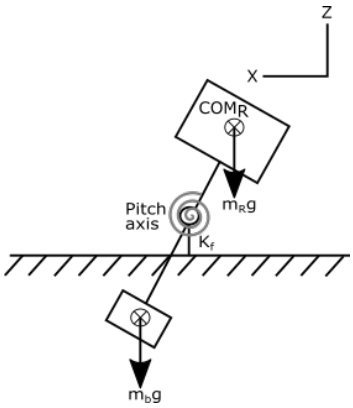

Figure 2.4: Free-body diagram of a robot allowed to rotate around a single axis. A counterbalance m_b and torsional spring k_f due to flexure stiffness cause a restoring moment to keep the robot's mass m_R to rest at a near-vertical inclination at equilibrium.

and flapping-wing platforms, pitch and roll torques can be actuated approximately independently. In a quad-rotor, if rotor speeds are changed, the resulting differential force between propellers causes a torque (Fig. 2.3). Roll torques in the FIRs are produced through a similar means, by increasing the thrust magnitude of one wing (T_1) relative to the other wing (T_2),

$$\tau_{roll} = (T_1 - T_2)b.$$

A pitch torque is produced by altering the position of the stroke-averaged center of aerodynamic thrust (Fig. 2.3),

$$\tau_{pitch} = (T_1 + T_2)d.$$

For a vehicle actuated by other means, such as four electrohydrodynamic thrusters [8] [7], actuation is very similar to quad-rotor devices.

2.4 Restoring Torque and Flexures

A flexure joint is a form of hinge that allows a rotation over a limited range [22]. Pin joints, bearings, and bushings are not suitable for small scale applications, due to friction scaling [23]. Ac-

cordingly, rotation in our trimming device is through flexure joints. A simplified, two-dimensional free-body diagram of the device is shown in Fig. 2.4. The resulting torque on the system, neglecting bias and trim torques, can be calculated using a moment balance and is equal to $k_f\theta - m_R g l_R \sin\theta + m_b g l_b \sin\theta$, where l_R and l_b are the moment arm of the robot and balancing weight from the pivot point respectively, k_f is the stiffness of the flexure joint, and m_R and m_b are the mass of the robot and counter-balance weight respectively. If we linearize the system using small-angle approximations around $\theta = 0$, we can write the equivalent stiffness as

$$k_s = k_f - m_R g l_R + m_b g l_b. \tag{2.5}$$

The restoring torque approaches zero as θ approaches zero. Therefore, for a properly-trimmed system ($\tau_b = \tau_t$), k_s does not play a role in trim torque calculations. For practical purposes, however, to ensure that the deflections due to typical bias torques can be measured from our motion capture cameras, k_s must not be too large. This is done by choosing the appropriate value of k_f.

In early exploratory investigations, we constructed a trimming device with a negative k_s, that is, without a counterbalance mass m_b. Under these conditions, the system did not have an equilibrium at θ but instead the robot rested at the limit of rotation, tilted. Under these conditions, the integral controller performed a "wind-up" until the integrated commanded torque exceeded what was necessary to drive the robot away from its tilted configuration. But with a negative spring constant, the required torque is maximum at that point, and the robot immediately flipped to the other tilted extreme. This repeated indefinitely back and forth as the integrator repeatedly wound up. This could be eliminated by adding a proportional component with the requisite spring-like restoring moment, but we chose the more expedient and practical solution of adding the balancing mass m_b. This had the additional advantage of allowing for the calibration step to eliminate O_R described in Section 3.4 below.

Chapter 3

TRIMMING A QUADCOPTER

Before doing experiment with FIRs we tested the concepts discussed in the previous chapter on a robot with comparatively slower dynamics like a quadcopter. Although, commercially available quadcopters have provisions for trimming, you can get a stable flight without trimming most of the times due to their slower dynamics and manufacturing consistencies in propeller systems. For this experiment we used Crazyflie [24], an open source quadcopter. We used the on-board IMU for the attitude measurements and on-board controller for calculating the trim values. Further, to introduce some inconsistencies in the propellers, propeller from one of the motor was clipped before doing the experiments.

3.1 Trimming Device for Quadcopter

Crazyflie is mounted on a set of two flexure joints as shown in 3.1, limiting its unconstrained degrees of freedom to two, pitch and roll. We chose flexures instead of pin joints because the same concept will be applied to the FIR and we wanted the setup to be similar. The flexures used here are made from thin polystyrene sheet sandwiched between two cardboards with thickness of 1.5mm. The two flexures (roll adn pitch flexure) are held together by a connecting plate made from same cardboard material with grooves perpendicular to each other on either side. Crazyflie is mounted on the setup using two 3 mm screws on the mounting holes of the robot. Equal weights were hanged from each side of the flexures to make the effective stiffness of the system positive by bringing the centre of mass of the system closer to the axis of rotation.

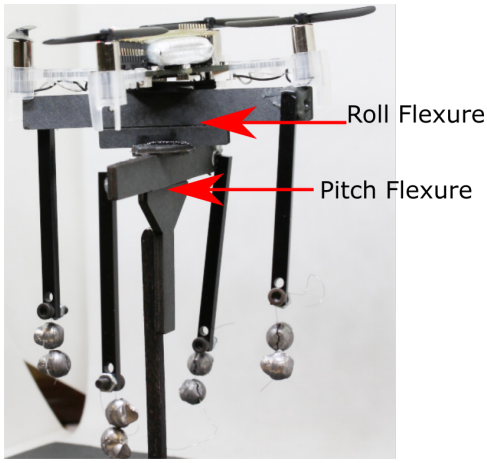

Figure 3.1: The experimental setup for the quad rotor to calculate the pitch and roll torque biases is shown here. The setup is made up of two flexure joints and balancing weights are used here to make the equivalent stiffness of the system positive.

3.2 Trimming Controller for Quadcopter

Roll and Pitch angles feedback is obtained form the IMU at the frequency of 100Hz. These angles are supplied as input to two independent integral controllers which estimate the trim values between -1 to 1. These values are then mapped to the motor speeds of the quadcopter, the sign of the trim value will signify which motor to adjust the speed on, while the value defines the percentage of PWM signal for that motor.

3.3 Trimming results for Quadcopter

The results from the trimming experiment on quadcopter are shown in Fig. 3.2. The robot started with an initial high attitude in pitch and roll, due to the clipped propeller, and slowly converged to zero pitch and roll angles. The obtained trim values map to the corresponding motor thrust percentage as $m1 = 100\%, m2 = 85\%, m3 = 100\%$, and $m4 = 95\%$. The analysis is done for a 10 seconds window in which the asymptotic stability of trimming values is achieved. This suggests the validity of principle of trimming using flexure joints.

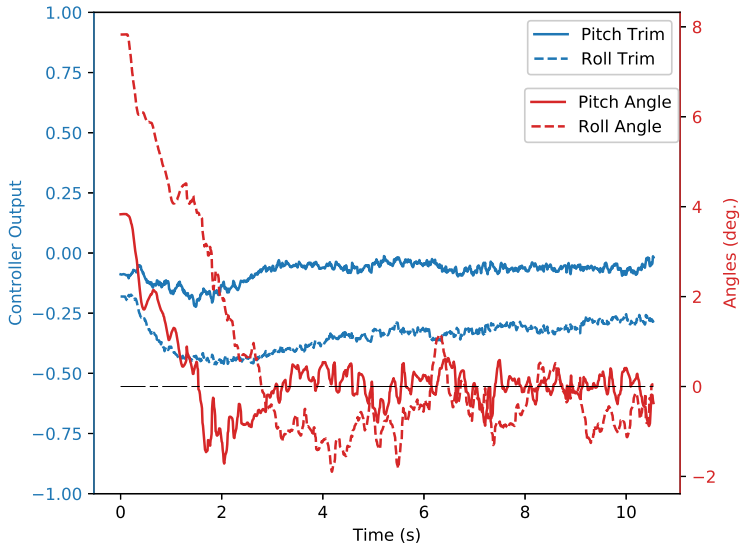

Figure 3.2: The results of trimming on a quadcopter with a clipped propeller are shown here. The initial pitch and roll angles were 4° and 8° respectively which converged to approximately 0° in 10 seconds. The corresponding trim values (blue) are obtained from this graph.

Chapter 4

TRIMMING A FLYING INSECT ROBOT

4.1 Experimental Apparatus

After validating the concepts introduced in chapter 2 on a quadcopter. The next step is build an apparatus which can perform the similar function of finding trim values on a flying insect robot. This chapter explains the design steps followed to build a trimming device and the results obtained by using that trimming device on Robofly-Expanded.

4.1.1 New Robot Design: Robofly-Expanded

As one of our contributions here, we introduce a new iteration of the Robofly design [1], called Robofly Expanded, that further simplifies fabrication. The new design integrates the wing hinge and legs directly into the main layup, reducing the part count for a complete Robofly, when legs are counted, from 12 in [1], to only 8, and far below the 18 of [2]. Additionally, the actuators are re-oriented so that their long axis is horizontal. This has two desirable results. First, by moving the wings farther apart from each other, torque around a vertical, or yaw axis is increased. This is necessary because the only known yaw actuation mode for this basic design consists of actuating the wing faster in one direction than the other to achieve a drag differential. However, this is known to produce a weak force [25]. Increasing the moment arm increases the net yaw force. In [5], this was shown to be sufficient to achieve consistent yaw actuation in either direction, something that was not possible in the design of [2]. Secondly, it allows for increased maneuverability in other directions, by orienting the long axis along the direction of greatest torque, the roll axis [21], and having a very little moment of inertia around its pitch axis. Measurements of pitch torque showed that they were substantially lower than roll torque, by a factor of approximately two [21]. A completed device is shown in Fig. 4.1.

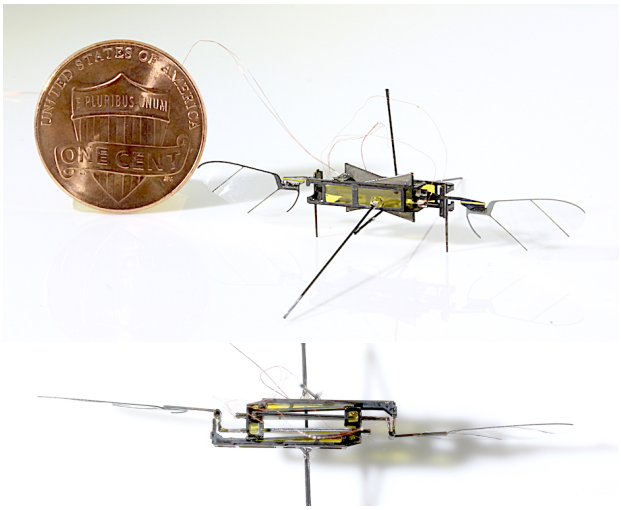

Figure 4.1: (top) We have redesigned the Robofly to simplify fabrication by further reducing the number of parts relative to [1] (U.S. penny coin shown for scale).

4.1.2 Trimming Device Design

We chose as our performance specification a maximum bias torque error of 0.3 μNm. This is motivated by the estimated torque uncertainty induced by the thin wire tether that provides power and control signals to the robot. While it is hard to provide a simple model of its effect due to its widely variable conformation, one reasonable model for the tether is a torsional spring. Experiments performed in [11] indicated that a 45° rotation causes a torque of approximately 0.3 μNm, leading to our performance target.

We then used our performance target to design the size of the flexure joints. Flexures were made of 12 μm polyimide film ("kapton"). The bending stiffness of the flexure joint, is calculated by using $k_f = \frac{Et^3w}{12L}$ [22]. Here, t is the thickness of the flexure material, L is the length of the flexure joint (500 μm), w is the width of the joint (3 mm) and E is Young's modulus of 2.5 Gpa. At these values, the resulting flexure stiffness is 2.16 μNm/rad. The same value of flexure stiffness is used for both roll and pitch joints. With this stiffness, a bias torque of 0.3 μNm produces a rotation of approximately 8°. This is easily measured by the motion capture arena, which can measure angles

to within approximately 1°, indicating that our device can provide the necessary accuracy. Note that we chose the counter-balance mass and position (Fig. 2.4) so that so that $m_b l_b \approx m_R l_R$ so that their equivalent stiffness counteracted the "negative stiffness" caused by the robot's COM being above the flexure rotation axis.

To mitigate buckling, all flexures were loaded in tension rather than compression. The remaining rigid structure was machined from inexpensive, rigid 254 μm fiberglass (FR4), which sandwiched the polyimide flexure material on both sides, following "smart composite microstructure" fabrication methods first introduced in [26]. A rigid part connects the two perpendicular pitch and roll flexures, which are designed so that their rotation axes are as close as possible to the robot's COM. Keeping that in mind the first iteration of the design (Fig. 4.4) kept this distance close to zero, but it was limited with the range of the laser. This impelled us to adopt to (Fig. 4.2 (b)), with distance 10 mm from COM of robot to the pitch axis. This can cause an error torque if the true thrust vector direction deviates from vertical, violating assumption 1. Adaptive controllers, e.g. in [2, 5], typically estimate this to be about 2°. This results in an error of approximately 0.3μNm, within the specification. This could be eliminated in a future revision that brings these flexures nearly perfectly coincident with the COM, but would require parts to physically surround the Robofly's wings, which extend farther than the $\approx$ 50 mm cutting range of the galvanometer of our laser machining system. The robot is mounted on the moving part of the pitch link through a connecting rod. The width of the roll link is minimized, at just 15 mm, so that it does not affect airflow from the wings.

4.1.3 Calibration/Positioning the Robot

Here we describe features of our trimming device that allow us to minimize O_R, the lateral displacement between the thrust vector and the trimming device's flexure-based rotation axis (Fig. 2.2(a)). Without this step, we found that trim estimates exhibited large errors, manifested in free-flight as large undesirable rotational accelerations at takeoff. To understand how a non-zero offset O_R could introduce error in our measurement, consider the case of robot displaced laterally by a small amount, such as O_R=1 mm, on the trimming device. If thrust T is equal to the mass of the vehi-

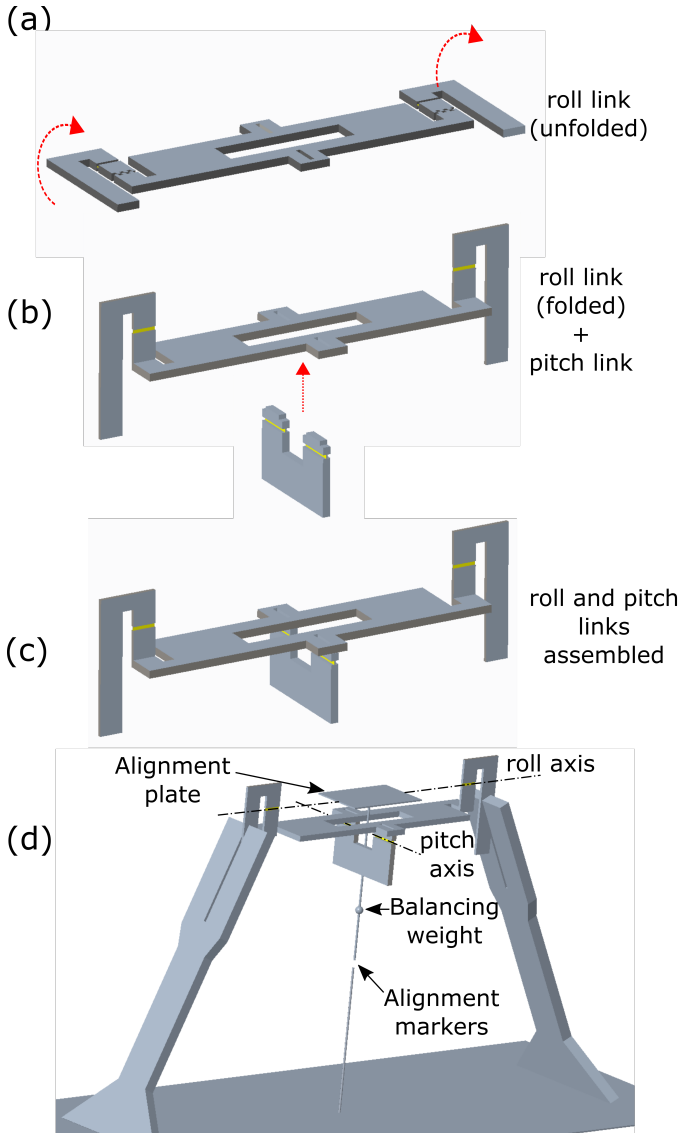

Figure 4.2: (a) The roll link of the trimming device. The link is folded around the castellated joint so the fly can be held perpendicular to the roll flexure and parallel to the ground. (b) The pitch link of the device. Its attached to the roll link via protrusions on top. (c) The whole assembly of trimming device, the fly is attached to the pitch link on the bottom. (d) Trimming device attached with the support columns, alignment fixtures and balancing weight.

cle, $T = mg$ = 1.2 mN, then the error in torque measurement $T \times O_R$ is 1.2 μNm. This is large compared our 0.3 μNm accuracy target, and therefore represents a source of error that must be eliminated.

Our solution is to use the mass of the robot itself as the source of information about its positioning. If the wings are not flapping, then a lateral displacement of its COM (O_R in Fig. 2.2(a)) induces a torque about the flexure due to gravity acting on the robot's body. Hence, the calibration procedure consists of moving the robot laterally on the the trimming device until its pitch and roll angles are equal to what they were before the robot was added (Fig. 4.3). After the robot is in its calibrated position, its feet are carefully glued to the surface with cyanoacrylate glue on a temporary basis. A soldering iron is used to carefully melt the glue and remove the robot when it is ready to fly.

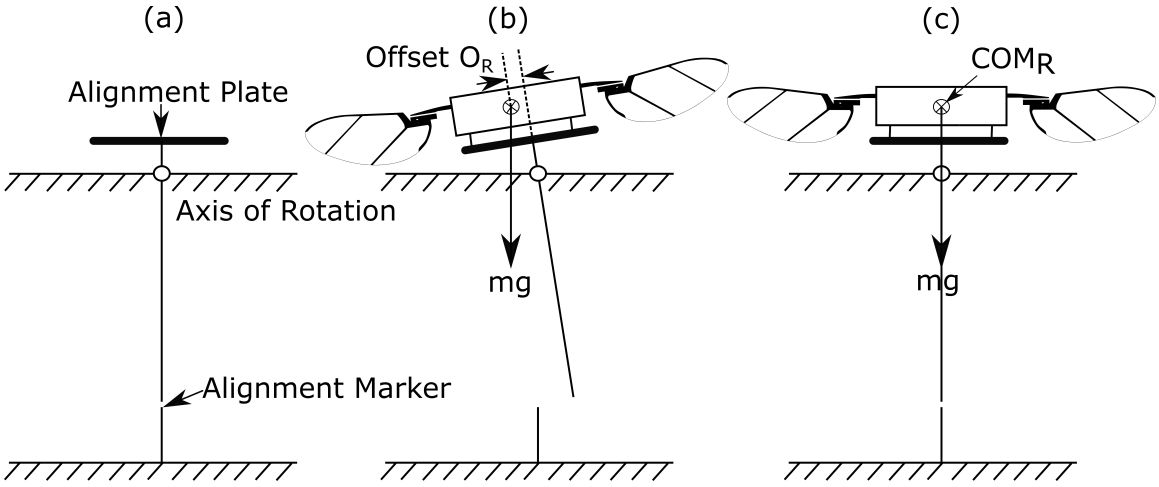

Figure 4.3: (a) To align the center of mass of the robot with axis of rotation of the device, we positioned an "alignment marker" just below a long rod. (b) The robot was then manually placed on a small "alignment plate" made of FR4 at the top of the connecting rod. Any lateral offset O_R causes rotation; the robot is carefully moved laterally in small increments with tweezers until the marks line up again for both pitch and roll axes, as shown in (c). This provides repeatability on the order of 1°.

4.1.4 Fabrication

Parts were machined using a diode-pumped solid state (DPSS) laser with a wavelength of 355 nM (Photomachining, Inc., Massachusetts). The roll link includes "castellated" cuts, which permit precise specification of the rotation axis, which are glued to a fixed angle as part of the assembly process (Fig. 4.2 (a)). Layers were pin-aligned and bonded together using a thermal sheet adhesive (18 μm Pyralux FR-1500) using a heat press at 200 C under a force of 50 kg. A subsequent release cut separated the required links from scaffolding. The assembly process is shown in Fig. 4.2 (b) in which the two links are glued together. These are bonded to a stable base that holds the assembly away from the surface of the table at about 15 cm to minimize the ground effect due to the table surface below. A lightweight scaffold is then added to hold the retroreflective motion capture markers. The complete device with a Robofly is shown in Fig. 4.5. In future, the trimming device can also be used for the characterization of torque response of the robot as a function of frequency. Its imperative to have a linear stiffness of the flexure joint in order to attain a consistent mapping between frequency and torque measurements. We loaded the pitch link (Fig 4.2(b)) with different static loads and noted the the deflection using a macro lens camera (Phantom v 5.1) to plot the data points in Fig. 4.6. The linear curve approximation of the data (Fig. 4.6(red)) has a mean squared error of 0.0027 rad suggesting the linearity in the stiffness of the flexure joints. The experimental value of stiffness obtained through this curve is 2.006 μNm which is consistent with its corresponding theoretical value.

4.1.5 Trimming Controller

A diagram showing the essential components of the closed-loop trimming system is shown in Fig. 4.7. The motion capture system (four Prime13 cameras, OptiTrack, Inc., Salem, OR) sends the orientation of the trimming device in quaternion form over Ethernet at 240 Hz. A computer running Simulink Real-Time (Mathworks, Natick, MA) performs control computations and produces an analog voltage waveform that is amplified using piezo amplifiers (Trek model 2205). The control computer calculates Euler angles roll θ_x and pitch θ_y from the quaternion, with a conven-

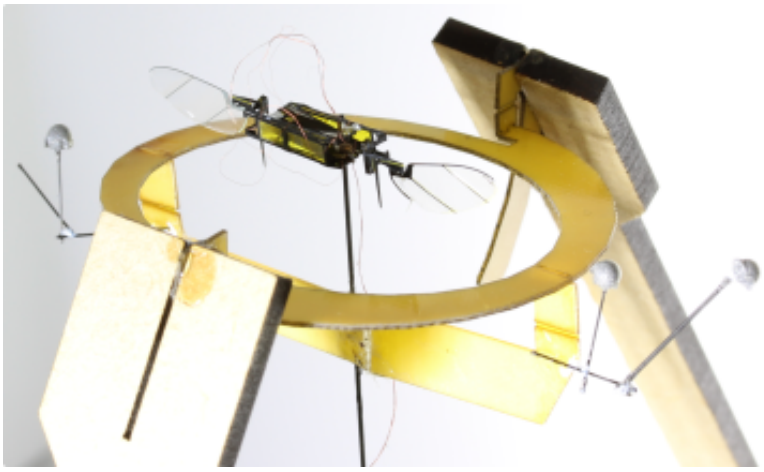

Figure 4.4: First iteration of the trimming device design. This design was made to keep the distance from COM of the robot to both the axis of rotation close to zero. However, this is limited by cutting range of the laser which impelled us to improvise this into a different design

tion matching those of the flexures in the trimming device. The displacement of the wings varies linearly with voltage applied to the piezo actuators, with the voltage signal to the left and right wings being

$$\begin{aligned} V_l(t) &= (A+\delta A)\sin(\omega t)+V_o \\ V_r(t) &= (A-\delta A)\sin(\omega t)+V_o, \end{aligned}$$

respectively. Thrust varies approximately linearly with flapping amplitude [27]. Here, A is the baseline voltage amplitude and ω is the flapping frequency. Roll torque is varied by varying δA, the amplitude difference between left and right wings. Pitch torque is varied by varying V_o, the mean voltage of the sinusoid. To avoid actuator breakage due to cracks, the controller includes saturation blocks to limit the range of these inputs [28].

4.2 Trimming Results

Voltage commands from the integral controller and output angles measured by motion capture for two different Robofly devices are shown in Fig. 4.8. In both cases, trim voltages appear to

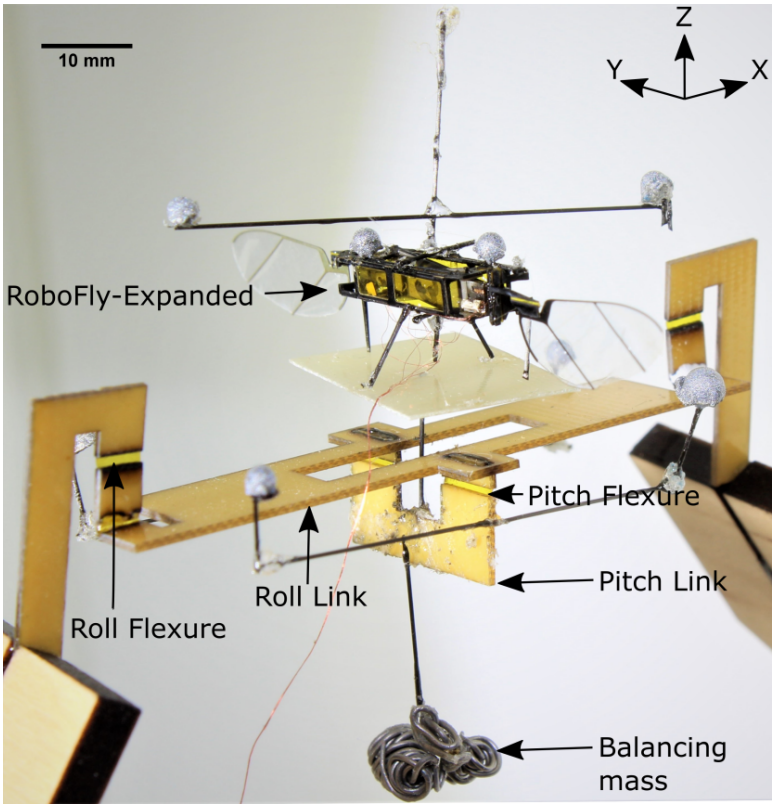

Figure 4.5: A Robofly is shown mounted on the reported trimming device. The device restricts all degrees of freedom except pitch and roll rotation, which occur through laser-microfabricated flexure joints joined by rigid links. A balancing mass at bottom insures that the system is at equilibrium in the upright orientation. Using this device, torque biases arising due to manufacturing irregularity can be detected and compensated for through an automated process.

asymptotically reach steady-state values within approximately 10 s. Resulting trim values are a pitch offset voltage V_o=-8 V and amplitude differential δA=3 V for the first and V_o=-5 V, δA=-17 V for the second. These results show that the system can arrive at a calibration regardless of the polarity of the bias torque.

To establish whether trimming was successful, we compared open-loop flights before and after trimming. In both cases, the wings were driven with a flapping frequency of 150 Hz and amplitude of 180 V. The device was constrained by a thin Kevlar thread to minimize crashes. For un-trimmed

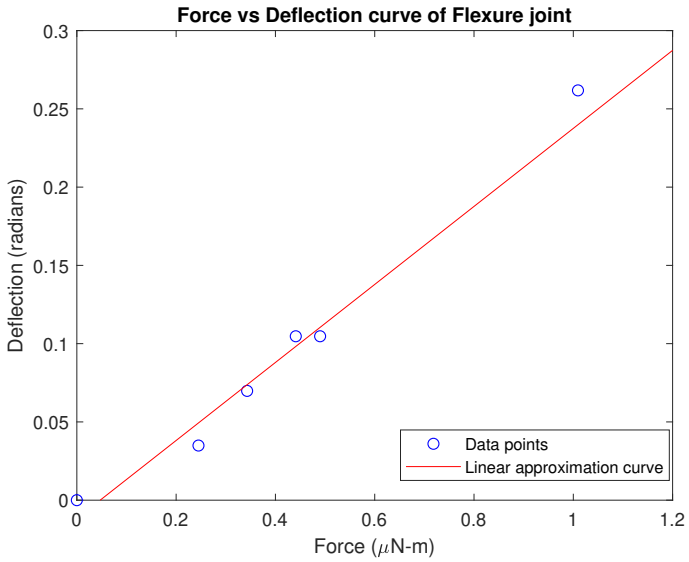

Figure 4.6: Deflection of the pitch link noted at different static loads (blue). The linear approximation of the data (red) has a mean square error of 0.0027 rad connoting the linearity in the stiffness of the flexure joints.

flights, $V_o = V_d = 0$. A video-composite of frames from an untrimmed flight shows that the robot exhibits large attitude deviation and soon flies out of the frame (Fig. 4.10 (a)). Using the trim voltages obtained from the trimming device, the robot can be observed to take off nearly vertically, indicating a properly-trimmed device (Fig. 4.10 (b)). The voltage signal used to drive the robot in Fig. 4.10 (b) is shown in Fig. 4.9. Similarly, the second Robofly exhibited an equivalent transition from tumbling to vertical flight after trimming.

4.3 Hovering

We confirmed that the trimming values from our trimming device could be used for hovering flight as well. We used the controller derived from the one in [5], which is an evolution of the one used in [2]. As in many controllers for underactuated systems, the controller operates by tilting the thrust vector in a desired direction to perform lateral motions [29, 5]. The first Robofly was commanded

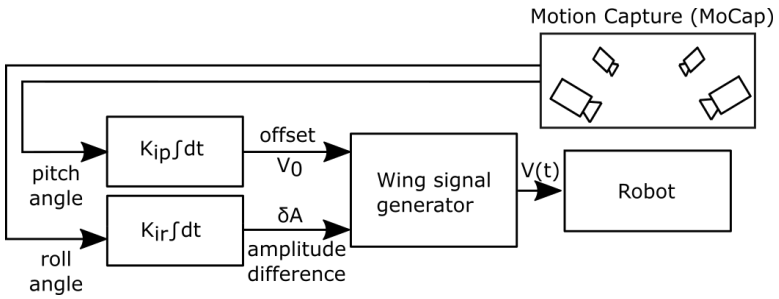

Figure 4.7: The control loop used in the trimming device generates the trim voltages by numerically integrating the error in roll and pitch angles estimated by motion capture cameras. The error signals are fed through a signal generator (Simulink real-time), converted to analog, amplified by piezo amplifiers, and fed to the piezo actuators driving the wings.

to hover at a height of 12 cm for 5 seconds. It was able to hover successfully using trim values from the trimming device with position RMS error of 21, 18 and 6 mm in x, y and z directions, respectively. The second Robofly also successfully hovered using its trim values from the trimming device at the height of 21 cm for 5 seconds with position RMS errors of 17, 49 and 7 mm in x, y and z directions respectively. The resulting 3D trajectories can be seen in the Fig. 4.13. Frames from the video are shown in Fig. 4.11 and Fig. 4.12. Videos of the trimming process on the device and open and closed-loop flights are provided in the supplementary video [30], as well as hovering results for both Roboflies tested.

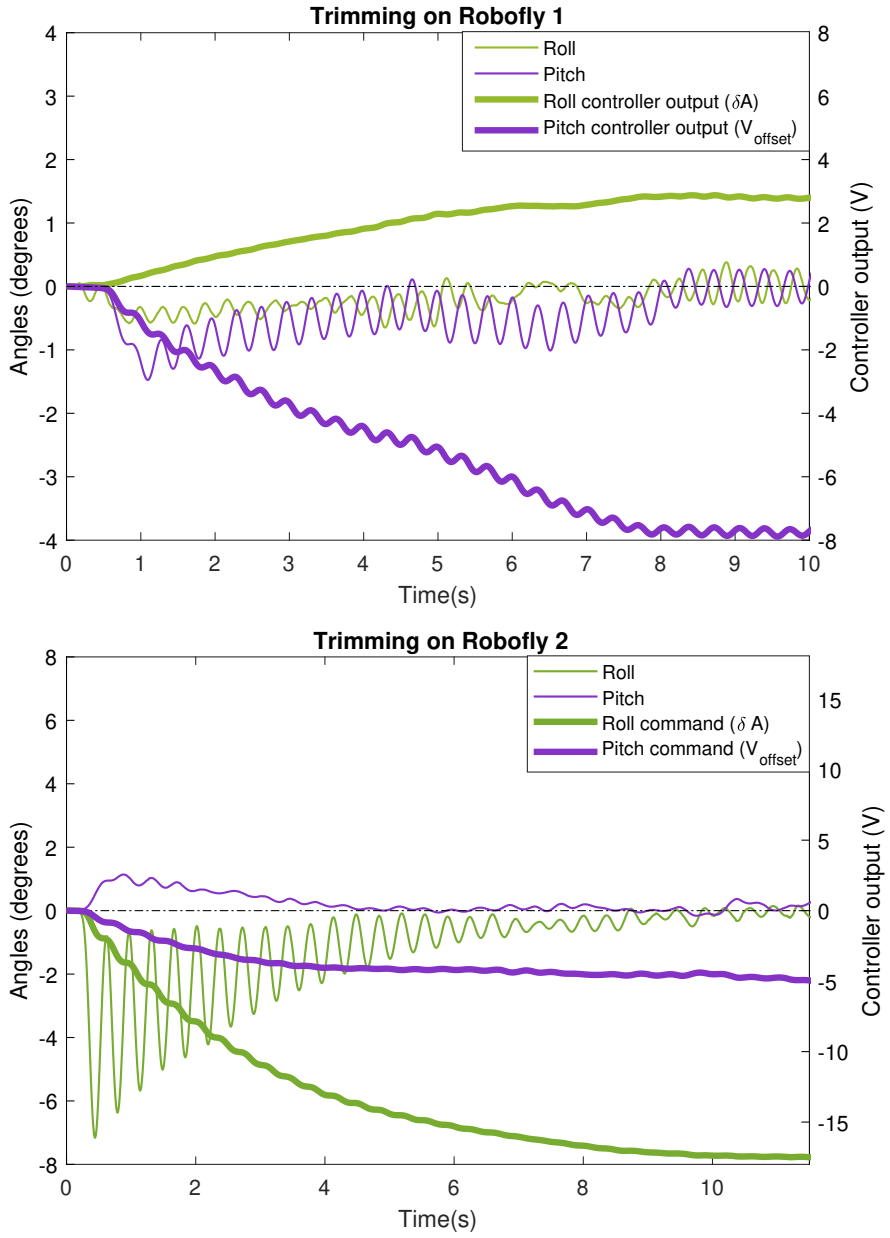

Figure 4.8: Results from trials on two different Robofly devices in the trimming device. Left axes show the angles of the two rotation axes as measured by motion capture, which are driven to zero by the integrating action of the feedback controller. Right axes show how the compensating bias voltages evolve in time as the trimming device settles on the correct trim values.

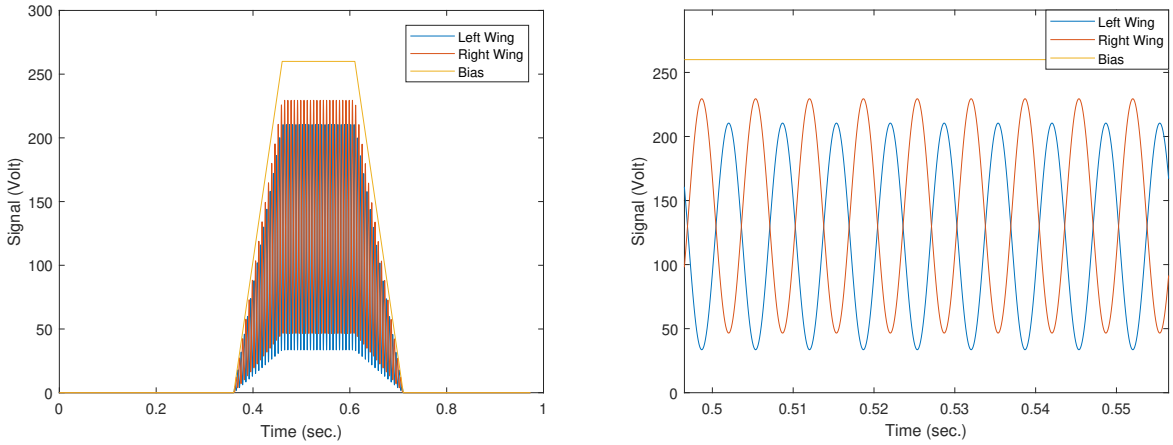

Figure 4.9: (left) Voltage signal after the trimming, given to each piezo-electric actuator for open-loop flight. The offset and amplitude of each signal is in accordance to controller output obtained by trimming.(Right) Same signal zoomed in for 0.05s , the offset and the differential amplitudes are clear in this graph.

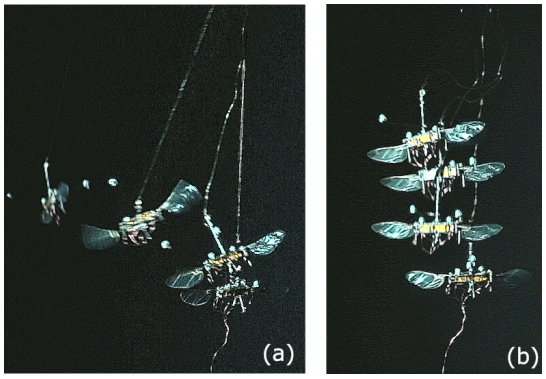

Figure 4.10: (a) Video-composite images taken from an un-trimmed open-loop takeoff of Robofly (offset voltage V_o and voltage differential δA at 0 V). (b) Open-loop of the same robot using trim values derived from the trimming device from the trimming procedure in Fig. 4.8(top). The robot lifts off nearly vertically, producing clearly-discernible slack in the kevlar restraining filament at the top. The vertical flight indicates that the vehicle has been properly trimmed.

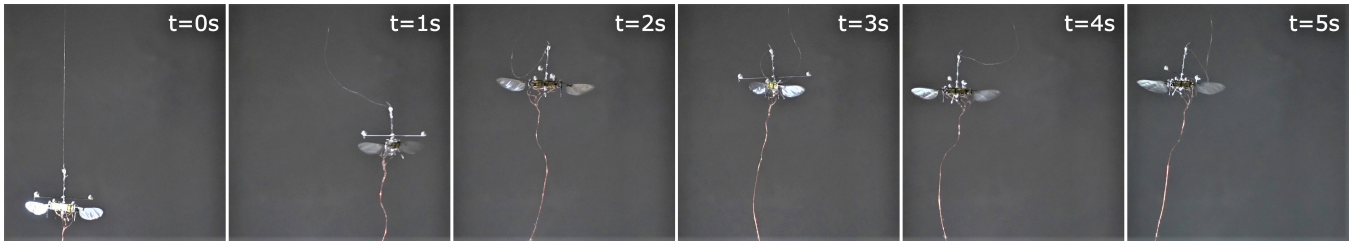

Figure 4.11: Snapshots of hovering Robot 1. The fly is controlled by an altitude and a lateral controller running in parallel. The trimming values used in the controller were obtained from the trimming device in the trimming procedure shown shown in Fig.4.8 (top).

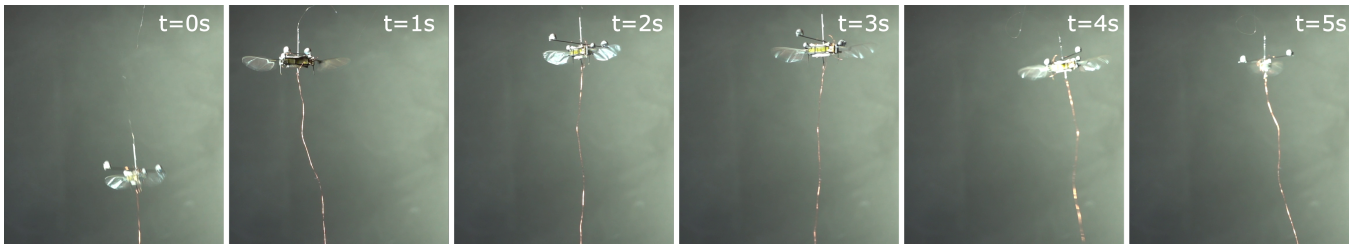

Figure 4.12: Snapshots of hovering Robot 2. The trimming values used in the controller were obtained from the trimming device in the trimming procedure shown shown in Fig.4.8 (bottom).

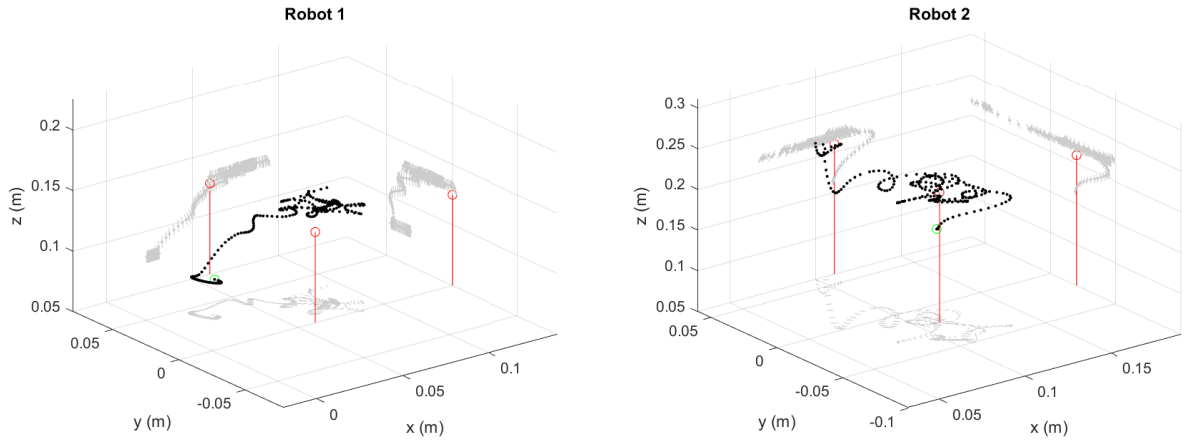

Figure 4.13: 3D trajectory of robots while hovering. The red circle shows the desired position in space. Black markers indicate the position of the robot spaced at intervals of 0.05 s. Projections of the trajectory, including its attitude, are shown in grey at the sides of the figure.

Chapter 5

CONCLUSION AND FUTURE WORK

5.1 Conclusion and Future Work

In this letter, we present a device for correcting the bias torques that are almost always present in small-sized airborne robots due to manufacturing irregularity in their complex flapping mechanics. Our device operates in a feedback control loop using motion capture feedback. We performed validation experiments on two different Robofly devices, successfully trimming them. In both cases, before the devices were trimmed, they exhibited strong pitch and roll torque in free flight, tumbling almost immediately after take-off. The entire trimming process took less than 25 minutes including calibration, and less than fifteen seconds of wing flapping time. Compared to manual trimming, where the trimming time and number of airborne flights depends on the operator skill, our process is automatic, more predictable and causes less wear. After trimming, both devices were observed to lift off nearly vertically and did not tumble. Trim values consisted of commanded voltage offsets to the drive waveform of the piezo actuators. Subsequently, we showed that our estimated trim values could be used by our controller to perform stable hovering flight. By greatly speeding and automating an essential yet time consuming step in robot fly fabrication, our device will facilitate high volume manufacturing of FIRs.

Our device is also able to trim robots with payload such as a battery or sensor package not perfectly centered relative to the COM. Misalignment is equivalent to a nonzero O_R that is corrected for using the calibration procedure in Fig. 4.3. An alternative way to build the trimming device is by tethering the robot to a thin metal rod. Although simple, this method would result in large estimation errors in the event that the thrust vector was not perfectly aligned with the body z-axis, because of the large moment arm.

Yaw trimming could be added by the incorporating a vertical-axis flexure between the align-

ment plate and connecting rod. This addition would not be subject to the potential for the confounding thrust-induced torque that required calibration for the pitch and roll axes, making it a simple addition. Furthermore, thrust force trimming could be added by placing the entire device on a sensitive balance scale, positioning the lightweight robot and trimming device off of the side of the scale to minimize aerodynamic ground effect. If the spring constant of is known, a full characterization of torque response as a function of frequency can be done using this device.

While our system was shown in operation on two-winged devices, its design accommodates other designs, such as 4-winged robots [5], or micro-robots actuated by other thruster types such as electrohydrodynamic thrusters [8].

The trimming device presented in this letter uses a camera-based motion capture system to measure orientation on the trimming device, but this is not a requirement. It is expected that most fully-autonomous robots will incorporate an inertial measurement unit (IMU) onboard [31]. The accelerometer in the IMU can serve as an inclinometer on the trimming device, precisely measuring the rotation angle for both pitch and roll axes in place of the motion capture system.

BIBLIOGRAPHY

[1] Y. M. Chukewad, A. T. Singh, J. M. James, and S. B. Fuller, "A new robot fly design that is easier to fabricate and capable of flight and ground locomotion," in *2018 IEEE/RSJ International Conference on Intelligent Robots and Systems (IROS)*. IEEE, 2018, pp. 4875–4882.

[2] K. Y. Ma, P. Chirarattananon, S. B. Fuller, and R. J. Wood, "Controlled flight of a biologically inspired, insect-scale robot," *Science*, vol. 340, no. 6132, pp. 603–607, 2013.

[3] H. V. Phan, Q. V. Nguyen, Q. T. Truong, T. Van Truong, H. C. Park, N. S. Goo, D. Byun, and M. J. Kim, "Stable vertical takeoff of an insect-mimicking flapping-wing system without guide implementing inherent pitching stability," *Journal of Bionic Engineering*, vol. 9, no. 4, pp. 391–401, 2012.

[4] C. T. Orlowski and A. R. Girard, "Dynamics, stability, and control analyses of flapping wing micro-air vehicles," *Progress in Aerospace Sciences*, vol. 51, pp. 18–30, 2012.

[5] S. B. Fuller, "Four wings: An insect-sized aerial robot with steering ability and payload capacity for autonomy," *IEEE Robotics and Automation Letters*, vol. 4, no. 2, pp. 570–577, 2019.

[6] X. Yang, Y. Chen, L. Chang, A. A. Calderón, and N. O. Pérez-Arancibia, "Bee$^+$: A 95-mg four-winged insect-scale flying robot driven by twinned unimorph actuators," *CoRR*, vol. abs/1905.02253, 2019. [Online]. Available: http://arxiv.org/abs/1905.02253

[7] D. S. Drew, N. O. Lambert, C. B. Schindler, and K. S. Pister, "Toward controlled flight of the ionocraft: a flying microrobot using electrohydrodynamic thrust with onboard sensing and no moving parts," *IEEE Robotics and Automation Letters*, vol. 3, no. 4, pp. 2807–2813, 2018.

[8] E. Dedic, Y. M. Chukewad, R. S. Vaddi, I. Novosselov, and S. B. Fuller, "A laser-microfabricated electrohydrodynamic thruster for centimeter-scale aerial robots," 2019.

[9] V. Kumar and N. Michael, "Opportunities and challenges with autonomous micro aerial vehicles," *The International Journal of Robotics Research*, vol. 31, no. 11, pp. 1279–1291, 2012.

[10] B. Cheng, X. Deng, and T. L. Hedrick, "The mechanics and control of pitching manoeuvres in a freely flying hawkmoth (manduca sexta)," *Journal of Experimental Biology*, vol. 214, no. 24, pp. 4092–4106, 2011.

[11] S. B. Fuller, M. Karpelson, A. Censi, K. Y. Ma, and R. J. Wood, "Controlling free flight of a robotic fly using an onboard vision sensor inspired by insect ocelli," *Journal of The Royal Society Interface*, vol. 11, no. 97, p. 20140281, 2014.

[12] S. Balasubramanian, Y. M. Chukewad, J. M. James, G. L. Barrows, and S. B. Fuller, "An insect-sized robot that uses a custom-built onboard camera and a neural network to classify and respond to visual input," in *2018 7th IEEE International Conference on Biomedical Robotics and Biomechatronics (Biorob)*. IEEE, 2018, pp. 1297–1302.

[13] J. James, V. Iyer, Y. Chukewad, S. Gollakota, and S. B. Fuller, "Liftoff of a 190 mg laser-powered aerial vehicle: The lightest wireless robot to fly," in *2018 IEEE International Conference on Robotics and Automation (ICRA)*. IEEE, 2018, pp. 1–8.

[14] N. Jafferis, E. Helbling, M. Karpelson, and R. Wood, "Untethered flight of an insect-sized flapping-wing microscale aerial vehicle," *Nature*, vol. 570, pp. 491–495, 06 2019.

[15] P. Chirarattananon, K. Y. Ma, and R. J. Wood, "Adaptive control for takeoff, hovering, and landing of a robotic fly," in *2013 IEEE/RSJ International Conference on Intelligent Robots and Systems*. IEEE, 2013, pp. 3808–3815.

[16] ——, "Adaptive control of a millimeter-scale flapping-wing robot," *Bioinspiration & biomimetics*, vol. 9, no. 2, p. 025004, 2014.

[17] D. Dhingra, Y. Chukewad, and S. B. Fuller, "A device for rapid, automated trimming of insect-sized flying robots," *IEEE Robotics and Automation Letters [under review]*, 2020.

[18] R. W. Yeung, "On the interactions of slender ships in shallow water," *Journal of Fluid Mechanics*, vol. 85, no. 1, pp. 143–159, 1978.

[19] R. C. Nelson *et al.*, *Flight stability and automatic control*. WCB/McGraw Hill New York, 1998, vol. 2.

[20] G. D. Padfield, *Helicopter flight dynamics*. Wiley Online Library, 2008.

[21] K. Y. Ma, S. M. Felton, and R. J. Wood, "Design, fabrication, and modeling of the split actuator microrobotic bee," in *2012 IEEE/RSJ International Conference on Intelligent Robots and Systems*. IEEE, 2012, pp. 1133–1140.

[22] R. Malka, A. L. Desbiens, Y. Chen, and R. J. Wood, "Principles of microscale flexure hinge design for enhanced endurance," in *2014 IEEE/RSJ International Conference on Intelligent Robots and Systems*. IEEE, 2014, pp. 2879–2885.

[23] R. J. Wood, B. M. Finio, M. Karpelson, K. Y. Ma, N. O. Pérez-Arancibia, P. S. Sreetharan, H. Tanaka, and J. P. Whitney, "Progress on "pico" air vehicles," in *ISRR*, 2011.

[24] [Online]. Available: https://wiki.bitcraze.io/projects:crazyflie:index

[25] N. Gravish and R. J. Wood, "Anomalous yaw torque generation from passively pitching wings," in *2016 IEEE International Conference on Robotics and Automation (ICRA)*. IEEE, 2016, pp. 3282–3287.

[26] A. M. Hoover, E. Steltz, and R. S. Fearing, "Roach: An autonomous 2.4 g crawling hexapod robot," in *2008 IEEE/RSJ International Conference on Intelligent Robots and Systems*. IEEE, 2008, pp. 26–33.

[27] N. O. Pérez-Arancibia, K. Y. Ma, K. C. Galloway, J. D. Greenberg, and R. J. Wood, "First controlled vertical flight of a biologically inspired microrobot," *Bioinspiration & Biomimetics*, vol. 6, no. 3, p. 036009, 2011.

[28] R. Wood, E. Steltz, and R. Fearing, "Optimal energy density piezoelectric bending actuators," *Sensors and Actuators A: Physical*, vol. 119, no. 2, pp. 476–488, 2005.

[29] A. Roberts and A. Tayebi, "Adaptive position tracking of vtol uavs," *IEEE Transactions on Robotics*, vol. 27, no. 1, pp. 129–142, 2010.

[30] [Online]. Available: https://youtu.be/-bCN2lxsMDs

[31] S. B. Fuller, E. F. Helbling, P. Chirarattananon, and R. J. Wood, "Using a mems gyroscope to stabilize the attitude of a fly-sized hovering robot," in *MAV 2014: Int. Micro Air Vehicle Conf.and Competition 2014, Delft, The Netherlands*. Citeseer, 2014.

[32] N. O. Pérez-Arancibia, K. Y. Ma, K. C. Galloway, J. D. Greenberg, and R. J. Wood, "First controlled vertical flight of a biologically inspired microrobot," *Bioinspiration and Biomimetics*, vol. 6, no. 3, p. 036009, Sep 2011.

[33] M. Sun and Y. Xiong, "Dynamic flight stability of a hovering bumblebee," *Journal of experimental biology*, vol. 208, no. 3, pp. 447–459, 2005.

[34] G. Taylor and A. Thomas, "Animal flight dynamics ii. longitudinal stability in flapping flight," *Journal of theoretical biology*, vol. 214, no. 3, pp. 351–370, 2002.

[35] M. Keennon, K. Klingebiel, and H. Won, "Development of the nano hummingbird: A tailless flapping wing micro air vehicle," in *50th AIAA aerospace sciences meeting including the new horizons forum and aerospace exposition*, 2012, p. 588.

[36] T. Bresciani, "Modelling, identification and control of a quadrotor helicopter," *MSc Theses*, 2008.

[37] D. A. Peters and D. Barwey, "A general theory of rotorcraft trim," *Mathematical Problems in Engineering*, vol. 2, no. 1, pp. 1–34, 1996.